Verification of a Mesoscale Data-Assimilation and Forecasting System for the Oklahoma City Area During the Joint Urban 2003 Field Project

Yubao Liu[1], Fei Chen[1], Thomas Warner[1,2] and Jeffrey Basara[3]

[1] National Center for Atmospheric Research*
Boulder, Colorado

[2] Program in Atmospheric and Oceanic Sciences
The University of Colorado
Boulder, Colorado

[3] Oklahoma Climate Survey, University of Oklahoma
Norman, Colorado

Submitted to
Journal of Applied Meteorology

May 2005

* The National Center for Atmospheric Research is principally sponsored by the National Science Foundation

Corresponding author:

Yubao Liu
NCAR/RAP
P.O. Box 3000
Boulder, Colorado 80307-3000
Phone:303/497-2811
Fax:303/497-8401
Email: yliu@ucar.edu

Abstract

The National Center for Atmospheric Research (NCAR) and the U.S. Army Test and Evaluation Command have developed a multi-scale, rapid-cycling, real-time, four-dimensional data-assimilation and forecasting system that has been in operational use at five Army test ranges since 2001. This system was employed to provide operational modeling support for the Joint Urban 2003 (JU2003) Dispersion Experiment, conducted in Oklahoma City during July 2003. To better support this mission, modifications were made to the non-local boundary-layer (BL) parameterization (known as the Medium Range Forecast scheme) of the Pennsylvania State University/NCAR Mesoscale Model, Version 5, in order to improve BL forecasts. The Noah land-surface model was also improved to better represent urban forcing. Verification of the operational model runs and retrospectively simulated cases shows 1) a significantly reduced low bias in the forecasted surface wind speed and 2) more-realistic daytime BL heights. During JU2003, the forecasted urban heat island, urban dry bubble, and urban BL height agree reasonably well with observations and conceptual models. An analysis of three-dimensional atmospheric structures, based on model analyses for eight clear-sky days during the field program, reveals some interesting features of the Oklahoma City urban BL, including complex thermally induced circulations and associated convergence/divergence zones, a nocturnal thermal shadow downwind of the urban area, and the reduction of low-level-jet wind speeds by more-vigorous nocturnal mixing over the city.

Keywords: urban numerical weather prediction, urban heat island, urban boundary layer, JU2003

1. Introduction

The National Center for Atmospheric Research (NCAR) has developed a Real-Time, multi-grid (grid increments of 0.5 - 45 km), Four-Dimensional Data Assimilation (RTFDDA) and forecasting system (Cram et al. 2001) for meteorological support of testing at U.S. Army Test and Evaluation Command (ATEC) test ranges. The RTFDDA system, based on the Pennsylvania State University/NCAR mesoscale model, Version 5 (MM5), has been running operationally at five Army test ranges for over four years. It is designed to cycle at a frequency of 1-12 h, with each cycle producing a model-based analysis and a forecast of up to 48 h duration. The data-assimilation system is based on Newtonian relaxation (Stauffer and Seaman 1994), and produces dynamically consistent model-assimilated data sets that are used as estimates of current conditions as well as for model initial conditions. In this paper, in addition to forecasts, analyses are verified against independent observations because they are important for providing input to short-range transport and diffusion (T&D) calculations. In addition to its use by the Army test ranges, the RTFDDA system has supported the missions of other Department of Defense (DOD) and government agencies.

In this paper is discussed the ability of the RTFDDA system to produce model-assimilated data sets and forecasts in support of the Joint Urban 2003 (JU2003) Atmospheric Dispersion Study, held in Oklahoma City (OKC), Oklahoma in July 2003. Even though the JU2003 study focused on building-scale effects on T&D in the central region of OKC (Allwine et al. 2004), accurate operational city-scale predictions of BL structures were needed for planning intensive observation periods. Therefore, during the

pre-JU2003 period, considerable effort was devoted to evaluating and improving MM5's data-assimilation methods and model-physics schemes in order to better represent the urban atmospheric environment. This paper describes two model improvements relevant to prediction of BL structures and urban effects. The first is related to MM5's commonly used Medium Range Forecast-model (MRF) BL parameterization (Hong and Pan 1996), and the second involves the representation of urban land-use/substrates in the Noah Land-Surface Model (LSM, Ek et al. 2003). As discussed in more detail in Section 2, most of the BL parameterization schemes available in MM5, including the MRF, tend to underestimate the daytime near-surface wind speeds. Also, the MRF scheme tends to develop the convective BL too early in the day, and it becomes excessively deep. Furthermore, the standard Noah LSM in MM5 (Chen and Dudhia 2001; Ek et al. 2003) has a simplified representation of cities, such that model tests showed only a very marginal Urban Heat Island (UHI) effect for OKC.

As with any moderate- to large-sized city, OKC has sufficient area that land-atmosphere interaction can affect the bulk, city-scale, dynamic and thermal evolution of the BL, and hence the T&D of airborne material over the city. Thus, correctly modeling the bulk urban effects on the atmosphere were crucial for the success of the RTFDDA system's support for this field experiment. There is much research aimed at understanding and modeling the complex land-atmosphere interaction that affects atmospheric dynamics and thermodynamics in urban areas, where methods involve field observations (Rotach 1995, Doran et al. 2002, Allwine et al. 2002) as well as parameterizing the processes in mesoscale models (Brown 2000, Grimmond and Oke 2002, Masson 2000). For example, using idealized environments, the improved

knowledge and modeling technology gained from the above and other studies have been used to investigate various aspects of the UHI, and urban-induced momentum mixing (Uno et al. 1989, Masson 2000, Grimmond and Oke 2002, Martilli et al. 2002, Dupont et al. 2003, Otte et al. 2004).

One approach for modeling the bulk effects of urban areas on the atmosphere is to use an urban canopy model (UCM, also known as urban canopy parameterization) to represent the model gridcell-averaged effect of the building structures on the dynamics and thermodynamics. Such UCMs parameterize the ensemble characteristics of the urban morphology, but individual buildings and street canyons are not explicitly represented (Brown 2000, Masson 2000, Martilli et al. 2002, Otte et al. 2004). At NCAR, an effort is underway to couple a UCM, that is based on the work of Kusaka et al. (2001), with the community mesoscale Weather Research and Forecasting (WRF) model (Chen et al. 2004). This type of UCM considers the geometry of building and roads to represent the radiation trapping and wind shear in the urban canopy. Such an approach requires detailed urban land-use data sets, and the input of a number of parameters that define the urban-geometry, where these parameters need to be calibrated for each individual city. In this operational support mission for the JU2003 field program, it was necessary to balance urban-model complexity and data-input requirements with the need to set up the model quickly. Therefore, we adopted an approach of modest complexity by which the Noah LSM in the public-release version of MM5 Version 3.4 was enhanced to capture the primary influences of the urban area (see Section 3 for details).

Section 2 describes the modifications made to the MRF BL parameterization, and in Section 3 the refinements to the Noah LSM are summarized. Section 4 contains an

objective verification of the improvements to the MRF BL parameterization. In Section 5 is a comparison of model products with field-program data, with Oklahoma mesonet data from locations surrounding the city, and with conceptual models of the urban BL. The last section, Section 6, provides a summary of this study.

2. Modification of the MM5 MRF BL parameterization

a. Known deficiencies with the current MRF BL parameterization

The MRF BL scheme, commonly used by the MM5 community for research and operational mesoscale weather forecasting, was selected for use in the RTFDDA system for its efficiency and its comparable overall performance relative to other BL schemes available in MM5. It is worth noting that the MRF parameters were defined by Hong and Pan (1996) using a single case, where the target was to improve coarse-resolution precipitation forecasts. A known problem with this parameterization has been that it tends to overestimate the daytime BL depth, and seriously underestimate the near-surface winds (Zhang and Zheng 2004). These problems can seriously impact the quality of T&D calculations that are based on MM5 output. For example, Cheng et al. (2003) reported that MM5 simulations with the MRF BL scheme persistently over-predicted the BL depth over the Houston-Galveston area. Also, in sensitivity experiments with five BL parameterizations available in MM5, for a period with three consecutive days of clear skies over the Central Plains, Zhang and Zheng (2004) found that all of the BL schemes underestimated the daytime near-surface winds, and that the MRF scheme performed the most poorly. They point out that there is a general lack of understanding of BL momentum-transport processes because previous research on BL and land-surface modeling has been primarily focused on thermal and moisture fluxes.

Statistical verification of the BL analyses and forecasts of the ATEC operational RTFDDA systems has revealed the same problem for various geographic regions and for all seasons. Figure 1 shows the bias errors of 10-m Above Ground Level (AGL) wind speed for 10-12 h forecasts on the fine mesh of a nested grid (1.1 or 3.3 km grid increment, depending on the ATEC range). These are averaged statistics for five test ranges, as verified against the range observations (total of 71 mesonet stations) during August 2002. Despite large geographic and climatic differences, the RTFDDA forecasts under-predicted the daytime wind speeds at all ranges.

In summer, the daytime BL is characterized by free-convective mixing of sensible and latent heat, as well as momentum. Winds near the surface are affected by the downward mixing of the higher momentum from above, and the upward mixing of lower momentum from below. Thus, an under-prediction of daytime near-surface winds can result from either an underestimate of the downward momentum flux, as speculated by Zhang and Zheng (2004), or an overestimate of surface stress.

As with most other BL parameterizations, the MRF scheme calculates the surface-layer fluxes based on Monin-Obukhov similarity theory (Beljaars, 1994), such that

$$\overline{\mathbf{W}'\theta'} = C_h|U|\,(\theta_{\mathbf{g}} - \theta_{\mathbf{a}}), \qquad (1)$$

$$\overline{\mathbf{W}'q'} = C_q|U|\,(q_{\mathbf{g}} - q_{\mathbf{a}}), \text{ and} \qquad (2)$$

$$\mathbf{u}_*^2 = C_m\,|U|^2, \qquad (3)$$

where $|\mathbf{U}|$ is the mean length of the horizontal wind vector ($\mathbf{U}^2 = u^2 + v^2$), and the subscripts **g** and **a** denote that the variables apply at ground-level (substrate surface) and

at the lowest model computation level, respectively. Other variables have their conventional meteorological meaning.

The extra eddy mixing induced by surface-layer free-convective instability is parameterized by replacing the mean horizontal wind $|\mathbf{U}|$ in Eqs. (1)-(3) with $\mathbf{U}_C$, which enhances $|\mathbf{U}|$ with a so-called convective velocity, $\mathbf{W}_*$ (Beljaars 1994):

$$\mathbf{U}_C^2 = U^2 + (\beta \mathbf{W}_*)^2. \qquad (4)$$

Physically, $\mathbf{U}_C$ represents the wind that is measured by a cup anemometer in free-convective conditions, and $\beta\mathbf{W}_*$ represents how much wind is measured in free-convective conditions when the large-scale wind is calm (Beljaars 1994). The inclusion of $\mathbf{W}_*$ in the surface mixing formulations enhances the surface heat and moisture fluxes, and increases the surface momentum consumption by turbulence.

In the standard MRF BL scheme, β is set to unity and $\mathbf{W}_*$ is computed based on the difference in the virtual potential temperature between the soil surface and the first model layer (Grell et al. 1993):

$$\mathbf{W}_* = \mathbf{C}\,(\theta_{\mathbf{vg}} - \theta_{\mathbf{va}})^{0.5}, \qquad (5)$$

where $\mathbf{C}$ is an empirical constant. The $\mathbf{W}_*$ formulation in (5) seems to represent the basic intended process. However, careful analysis exposes a few problems with this formulation. First, the depth of the lowest model layer, which determines where $\theta_{\mathbf{va}}$ is defined, will affect the $\mathbf{W}_*$ calculation, and this depth varies significantly from one model

application to another. In addition, with the sigma vertical coordinate used in the MM5 model, the depths of the model layers, especially the lower ones, vary horizontally with terrain height. Also, different soil models often have alternative ways of defining "surface" or "skin" temperature, resulting in a significantly different virtual potential temperature at the surface (θ_{vg}). For example, in a SLAB soil model (Zhang and Anthes 1982), the "skin" is represented by an uppermost soil layer of finite thickness, whereas in the Noah land-surface model the "skin" represents the infinitely thin layer at the top of the soil. This could typically result in a difference of ~10 K in θ_{vg}, and seriously affect the estimate of $\mathbf{W}_*$. Although the parameter **C** may be adjusted for different weather scenarios, this approach cannot deal with the many complexities mentioned above. In fact, the parameter **C** was set to 2.0 many years ago in the MM5 system (Grell et al. 1993), when only the SLAB soil model was available, and has since remained unchanged. This setting, of course, is not compatible with the modern MM5 systems, where the Oregon State University and Noah LSMs are used, and a very thin lowest model layer is typically used for the atmosphere.

An analysis of RTFDDA results confirms the problem with the $\mathbf{W}_*$ formulation in Eq. (5). On a typical summer day with clear skies, MM5 simulations, with the Noah LSM scheme and the lowest model computation level at ~15 m AGL, can produce differences in θ_{vg} and θ_{va} of 10 - 25 C during the daytime. For a difference of 16 C, Eq. (5) will yield a $\mathbf{W}_*$ of about 8 m s^{-1}, which is larger than $|\mathbf{U}|$ in most weather situations. This difference will lead to an overestimate of the friction velocity ($\mathbf{u}_*$), resulting in excessively weak near-surface winds. And, unfortunately, with the excessively weak near-surface winds,

the free-convective mixing ($\mathbf{W}_*$) becomes, relatively speaking, even more dominant in the surface-layer flux computation.

b. Incorporating Beljaars' formulation into the MRF BL parameterization

To better represent convective velocities, a more sophisticated surface-flux formulation (Beljaars 1994 and Deardorff 1970) was implemented into the MRF BL scheme for the OKC modeling. In Beljaars' formulation, $\mathbf{W}_*$ is computed directly from the surface sensible- and latent-heat fluxes, and the BL height:

$$\mathbf{W}_* = (\mathbf{z}_i \, \overline{W'\theta'_v} \, g/T)^{1/3}, \qquad (6)$$

where $\mathbf{z}_i$ is the BL depth, g/T represents buoyancy, and $\overline{\mathbf{W}'\theta'_v}$ is the sum of the surface sensible and latent heat fluxes ($\overline{\mathbf{W}'\theta'_v} = \overline{W'\theta'} + 0.61\theta_v\overline{W'q'}$). This new $\mathbf{W}_*$ formulation is more physically based because the $\mathbf{W}_*$ is directly linked to the heat flux and BL depth, which are related to the strength of the convective turbulence. Unlike in Eq. (5), the $\mathbf{W}_*$ formulation in Eq. (6) does not depend on a tuning parameter, the specification of the lowest model-layer depth, and the definition of the soil skin. Furthermore, in Beljaars (1994), the β coefficient (Eq. 4) of the $\mathbf{W}_*$ formulation in Eq. (6) was calibrated with an LES simulation by Sykes et al. (1993). According to Beljaars' calibration, β varies with the BL depth between 0.8 and 1.3, from deep to shallow BLs. In these RTFDDA applications, β is set at 1.1.

c. A new method for calculating the BL height

From Eq. (6), an accurate computation of $\mathbf{W}_*$ will still rely on estimates of the BL depth, as well as the surface heat and moisture fluxes. Recall that one of the known problems with the original MRF BL scheme is its overestimate of the BL height. Analysis of the RTFDDA output indicates that the MRF BL scheme frequently produces premature BL development (1-3 h), that results in excessively deep BLs (by a few hundred meters to more than 1 km) in the morning. These BL-depth errors not only affect the BL thermodynamic structure, but also directly result in an overestimate of $\mathbf{W}_*$. In order to improve the surface-flux computation in the free-convective BL, the MRF BL depth needed to be improved.

In the original MRF BL scheme, the BL height is diagnosed with a bulk Richardson number ($\mathbf{R}i_b$) that is defined over a layer between the surface (k_s) and a model level (k) above,

$$Ri_b(k) = \frac{gh(\theta_v(k) - \theta_v(k_s)}{\theta_v(k)(U(k))^2}.$$

The BL height is defined by comparing the $\mathbf{R}i_b$ with the critical Richardson number ($\mathbf{R}i_c$), which is set at 0.25. Searching from the bottom up, when the $\mathbf{R}i_b$ of the layer between the surface and a model level is found to be larger than $\mathbf{R}i_c$, the BL height is defined to be equal to the height of the model level, plus an increment that is calculated by an upward extrapolation according to the difference between the $\mathbf{R}i_b$ and $\mathbf{R}i_c$. This approach seems consistent with the non-local mixing strategy of the MRF BL scheme. However it is subject to a few problems. First, wind shear may vary greatly with height in the lowest 1-3 km, and sometimes wind maxima can be observed within a BL. Second, there exist phase (time) lags between the evolution of the surface thermal state and the BL structure, and therefore the model surface thermal state may be subject to some phase and/or

amplitude errors. Thus, the $\mathbf{Ri}_b$ in a layer between the surface and a model level above may not be a good indicator of the turbulence in the layer. And, the $\mathbf{Ri}_b$ may not represent the turbulence near the BL top at all. Thus, using $\mathbf{Ri}_b$ to define the BL height will by no means be accurate.

A new approach is introduced to improve the BL-height calculation. Instead of using the deep-layer $\mathbf{Ri}_b$, the new approach estimates BL heights by using a local bulk Richardson number ($\mathbf{Ri}_{bl}$), say at model level k,

$$Ri_{bl}(k) = \frac{2g\Delta h(\theta_v(k+1) - \theta_v(k)}{(\theta_v(k+1) + \theta_v(k))(U(k+1) - U(k))^2}.$$

The $\mathbf{Ri}_{bl}$ is computed for each model layer based on the wind shear and thermal stability between two neighboring model levels. Like the old approach, the BL height is determined by searching from the bottom up. When $\mathbf{Ri}_{bl} > \mathbf{Ri}_c$ is found for a model layer, the BL height is set to the height of the top of the layer, plus an adjustment obtained by using the same extrapolation method as before. In contrast to the $\mathbf{Ri}_b$, the $\mathbf{Ri}_{bl}$ represents the local state of the model layers in the model BL, and thus can better trace the BL development. This new BL-height computation is less sensitive to short-lived changes in the surface thermal state.

It is of interest to point out that, using the $\mathbf{Ri}_{bl}$ to estimate BL heights is conceptually consistent with the approach in more-complicated, higher-order BL turbulence-closure schemes, where BL heights are diagnosed based on turbulence kinetic energy (TKE) which is predicted at the model grid points. These local TKE values represent the intensity of the local turbulence, which is similar to using the $\mathbf{Ri}_{bl}$. Numerical experiments run on the same cases with different BL parameterizations showed that the BL heights calculated with the revised MRF BL scheme are very close to

those diagnosed by the more sophisticated and computationally demanding Meller-Yamada-Janjic TKE scheme (not shown).

Finally, it is noted that the Noah LSM uses a skin temperature, for heat transfer calculations, that is defined at the ground surface, and not at the height of the roughness length. Hence, the Monin-Obukhov similarity theory cannot be directly applied. The effect of the molecular sub-layer is to act as a resistance to fluxes, and it is equivalent in this sense to a thermal roughness length that is smaller than the roughness length for momentum. Zilitinkevich (1995) proposed relating this ratio to the roughness Reynolds number, and Chen et al. (1997) found that this approach can improve the surface heat flux and skin temperature simulations. This scheme was introduced into MM5 by Chen and Dudhia (2001). It is restated here because it is of great importance to incorporate this refinement along with the MRF BL modifications described previously.

3. Modification to the representation of urban areas in the Noah LSM

Properly modeling urban effects on the atmosphere was crucial for the success of the use of RTFDDA to support the JU2003 experiment. In the model configuration used, the urban area occupied roughly 20% of the 1.5-km grid and 70% of the 0.5-km grid (see Fig.2). At this horizontal resolution, the bulk influence of the urban land-surface forcing on the BL should be representable, as should effects related to the irregular shape of the urban area. Niyogi et al. (1999) and Holt et al. (2005) indicate the importance of small-scale land-surface heterogeneity to BL development. Although urban parameterization schemes with varying degrees of complexity have been coupled to many versions of MM5 (Otte et al. 2004, Dupont et al. 2003, Brown 2000), they are not yet available in the

public release of MM5. In addition, it is not clear what level of complexity in the urban land-use treatment should be incorporated. For instance, Taha (1999) prefers a simple approach, and points out that a large amount of detail in complex urban models may be lost when averaging back to a coarse model grid. Eventually, the WRF Noah LSM will be coupled with an advanced, one-layer, urban-canopy model (UCM) that is based on Kusaka et al. (2001). For the work described here, a simple bulk representation of urban areas was incorporated in the standard MM5 and WRF Noah LSM (Chen and Dudhia 2001). Given the simplicity, efficient computations, and encouraging results (shown below) of these improvements to the Noah LSM, we believe this relatively simple approach could be a good alternative to the more complex UCM for operational forecasting for urban areas on these scales. In fact, the modifications introduced here are already being used by others (Grossman-Clarke et al. 2005; Daewon Byun, personal communication; David Stauffer, personal communication).

The Noah LSM urban enhancements include increasing the roughness length from 0.5 m to 0.8 m to better account for the drag due to buildings. The roughness length of 0.8 m used here is slightly lower than the 1.0 m used by Atkinson (2003), in consideration of the generally low buildings in OKC. The surface albedo was reduced from 0.18 to 0.15, where this reduction accounted for the shortwave radiation trapping in the urban canyons (The new value is consistent with the average for urban areas suggested by Pielke 1984, and the same value was suggested by Atkinson 2003). The volumetric heat capacity was increased to 3.0×10^6 J m^{-3} K^{-1} and the soil thermal conductivity to 3.24 W m^{-1} K^{-1}. These two values are larger than those for the prevailing concrete/asphalt materials (about 2.0×10^6 J m^{-3} K^{-1} and 2.0 W m^{-1} K^{-1}, respectively), to

roughly reflect the heat storage due to building walls. Lastly, the green vegetation fraction was reduced to 0.05, and the available urban soil-water capacity was decreased to reduce evaporation. At present, there is no proper estimate of the bulk water capacity in urban regions. We adjusted these parameters experimentally, prior to the RTFDDA support for the JU2003, to keep the surface latent-heat flux small when there is no rain. In a few UHI models (e.g., Martilli et al. 2002 and Otte et al. 2004), the surface evaporation is ignored. Note that these physical properties were not chosen to "tune" the model solutions to the JU2003 field program data and other data used in this study; they were based on estimates made prior to the verification process.

4. Pre-field-program verification of the performance of the improved MRF BL parameterization

Testing of the modified MRF BL scheme and Noah LSM was conducted during the preparation stage for the JU2003 field experiment. Thus, data sets that were available prior to the experiment are used here for verification.

a. Verification during a three-day period in the Central Plains: 26-28 May 2003

A period with clear skies over the Central Plains, from 26-28 May 2003, was chosen because of the strong growth of the BL. Five nested-grids were used, with grid increments of 40.5, 13.5, 4.5, 1.5 and 0.5 km (Fig.2). The RTFDDA system was cycled every 3 h, and for each cycle a final analysis of present conditions and a 15-h forecast were generated. The model physics, aside from the modified MRF BL, were the same as those described in Liu et al. (2002). The RTFDDA analyses and forecasts were verified

against hourly near-surface observations and 12-hourly radiosondes. Here, only the surface verification of the analyses and 10-12 h forecasts are presented.

First, simulations were conducted to verify the new BL-height calculation scheme. The RTFDDA-forecasted BL heights for 0500-1800 Local Time (LT) 28 May 2003, calculated using the new and old (original) methods, were interpolated from model Domain 1 to the locations of three profilers located in Kansas and operated by the Argonne National Laboratory (ANL). The low-power, signal-to-noise ratio (SNR) of the wind profilers may be used to infer BL turbulence properties. Coulter and Holdridge (1998) and LeMone et al. (2000) describe how to define BL heights according to the values and vertical gradient of the SNR. Essentially, the BL heights are located immediately above the maximum in the vertical gradient of the SNR. It should be noted that, because the SNR is dependent on local moisture gradients, the estimates may differ from the real BL height in some instances, e.g. during the late afternoon when the BL is collapsing. Thus, one needs to be cautious when estimating the BL height with the wind profiler SNR returns. Figure 3 shows the comparison of the BL-height evolution of the RTFDDA model runs, with the old and new BL schemes, and SNR fields from ANL profilers located at Beaumont, Whitewater, and Oxford, Kansas. The BL height calculated with the original approach develops too early, and becomes too deep during the daytime. In contrast, the new approach performs better, even though, arguably, the BL heights are under-predicted in the early afternoon.

Next, a comparison was conducted of the performance of the old and the new MRF BL schemes for the period 0000 UTC 27 May to 0000 UTC 29 May 2003. Figure 4 shows the verification of 10-m AGL, 10-12 h wind-speed forecasts from the two model

versions, based on over 1400 METAR and other near-surface observations on model Domain 1 for the series of forecasts initiated every 3 h over the three-day period. Again, values were interpolated from the model grid to the locations of the observations. The original scheme considerably underestimated daytime 10-m AGL winds, with a maximum bias of -2.5 m s^{-1} occurring at about 1500 LT for the 10-12 h forecasts and a maximum bias of -1.6 m s^{-1} during the day for the analyses (Fig. 4a). The wind-speed RMS errors (Fig. 4b) have maxima during the day. The modified MRF BL scheme reduces these daytime weak-wind forecast biases by more than 70% at some times. In addition, the new scheme also improved, albeit to a lesser degree, the nocturnal wind-speed forecast. With the revised MRF BL scheme, the RMS errors during the night and day are of similar magnitude.

Although the major goal of the MRF BL modification was to correct the daytime weak-wind bias near the surface, the other near-surface variables also benefit to a lesser degree. Figure 5 shows that the new scheme improves the daytime and early-evening 10-m AGL wind-direction and 2-m AGL temperature predictions. At some times, the wind direction is improved by 10 degrees. Humidity forecasts have a similar improvement (not shown). Verification of forecasts from the finer grid meshes (Fig. 2) shows improvements very similar to those just described for Domain 1.

b. Verification for Aberdeen, Maryland, for a one-month period

In contrast to the above evaluation of the modified MRF BL scheme for a few case-study days, in this section we examine its performance in the context of an operational mesoscale forecasting system at the ATEC Aberdeen Test Center, Maryland. Statistics for the month of August 2002, before the changes were made, are compared

with those for August 2003, after they were made. Figure 6 compares the monthly mean, 10-m AGL wind-speed bias and RMS errors on the middle grid of a three-grid nest, where the grid increment is 10 km. Again, the verification is done by interpolating the model output to all surface stations. As with the previous case-study results, Fig. 6a shows a significant improvement in the 10-m AGL daytime wind-speed bias with the new MRF BL, with the monthly mean, 4-6 h forecast biases for 1200 LT decreasing from 2.2 m s^{-1} to 0.5 m s^{-1}. Similar improvements can be seen in the daytime RMS wind-speed errors in Fig. 6b, with nighttime benefits also being evident. Other variables show improvements similar to those computed for the case studies above.

5. Application of the enhanced model to the JU2003 field-program period, and assessment of performance

In this section, analyses from the enhanced model are compared with data for the JU2003 field-program period, and the ability of the model to replicate observed BL properties is assessed. Note that it is reasonable to employ model-generated analyses because the field-program data with which they are compared were not assimilated in the operational system. Because urban effects are more identifiable during clear days with weak synoptic forcing, model verification in this section focuses on eight clear-sky days (4, 5, 15, 16, 17, 18, 24 and 25 July) during that period.

a. Verification of near-surface variables

Verification data used here are from the JU2003 field program and the Oklahoma Mesonet (Brock et al. 1995). Three observation stations were selected for use (Fig. 2): PW14 (PWIDS 14) represents an urban setting, and the sensor is mounted on a light pole

in the central OKC business district. The PWIDS (Portable Weather Information Display System) is a light weight mobile surface atmospheric measurement station. It measures wind speed, wind direction, temperature and relative humidity. The SPEN station is in the suburbs to the northeast of the city; and MINC represents rural conditions and is to the southwest of the city. The PW14 station was operated by the U.S. Army Dugway Proving Ground for the field program, and SPEN and MINC are permanent Oklahoma Mesonetwork stations (Brock et al. 1995) . The model near-surface variables on Domain 4 were interpolated to the station locations. The prevailing surface flow over the OKC region is typically from the south in July, and this was the case for all the clear-sky days used here, except for 24 July on which a northeasterly to southeasterly flow was observed. The following subsections describe comparisons of simulated and observed temperature and specific humidity. Model winds are not verified here because the measurement location in the urban area is within a street canyon, and thus the data are not representative of the scales that are simulated by the model

1) Near-surface temperature

The diurnal evolution of the observed and model analyzed 10-m AGL temperatures at the three stations is presented in Fig. 7 for 16 July (southerly flow) and 24 July (easterly flow) 2003. The verification results for the other six clear-sky days are generally similar to those for the 16 July case. Also, Table 1 presents, for each of the eight dates, the observed and predicted 1) amplitude of the diurnal temperature variation and 2) urban-rural and urban-suburban temperature differences for 0600 LT and 1400 LT. The 1400 LT time was chosen to reflect conditions in the warm BL because precipitation was observed late in the afternoon for a few of the cases, and that locally influenced

temperatures. The following general conclusions about model performance can be obtained from Fig. 7 and Table 1.

- The timing of the simulated and observed temperature minima and maxima coincide well (Fig. 7). The observed mid-morning small difference in the temperatures among the three locations is generally represented by the model (Fig. 7). The small mid-morning urban-rural temperature difference is a well-document phenomenon (Oke 1987). After sunrises, urban regions heat up more slowly than rural areas because of the larger heat capacity and conductivity of the urban surface.
- The diurnal temperature ranges were simulated well (Table 1 and Fig. 7). For each of the three locations, 24 July had the largest observed and forecasted diurnal range of the eight days. And, for 5 July the model correctly forecasted the smallest diurnal amplitude of the eight days at all three of the locations. Also, the ranking of the three locations in terms of the eight-day-average diurnal range is the same based on the model and the observations: The rural location had the largest, the suburban location had the smallest, and the urban site was intermediate. Individual errors were frequently in the range of a few tenths of a degree, with the average error being 0.5-0.6 C, or about 5% of the observed range.
- The simulated temperature excess of the urban site relative to the other two non-urban sites (the UHI) is reasonable for most days at the indicated times, but the error can occasionally be significant (Table 1). For example, on the three days out of the eight with the largest observed urban-rural nocturnal-UHI temperature excess (16, 17, and 18 July), the model also predicted the largest UHI effect. The

UHI effect is correctly simulated to be larger at night (2.0-4.0 C urban-rural difference), relative to other times of the day (1.0-2.5 C during the day). The simulated urban-rural temperature difference, averaged over the seven days with southerly flow, is 2.54 C, only 0.11 C less than observed. Forecasts with misplaced isolated precipitation were occasionally responsible for temperature errors.

- The observations show that the nocturnal temperature at the rural site is warmer than that at the suburban site on 24 July, whereas the observed relationship has the opposite sign on 16 July (Fig. 7) and the other six days. The model captured the reversal on this day. On the 24th, the observed and predicted large-scale winds veered during the night from northeasterly to southeasterly, which meant that the rural site to the southwest of the city could have been influenced by the advection of the UHI warm anomaly, the "thermal shadow", and therefore remained warmer than the upwind suburban location.
- The forecasted temperatures have a 1-3 C positive bias (Fig. 7).

It is encouraging that the model simulations verified reasonably well in spite of the fact that conventional Eta-model soil-moisture and -temperature fields were used to initialize RTFDDA, and the complexities of the urban radiation budget were not seriously treated.

2) Near-surface humidity

Relative-humidity (RH) differences between urban and rural areas result from both the UHI effect and specific-humidity differences. Because of strong city-to-city variability in the amplitude of the UHI effect, it is difficult to state a typical urban-rural RH contrast. However, observations for individual cities have shown contrasts that vary

from 5 to 30%, depending on season and time of day. For the dates studied here, eight-day-average observed and simulated, 10-m urban RH deficits (relative to the rural location) are 16% and 14%, respectively, for 0600 LT. Specific humidity derived from JU2003 observations shows the urban location to be 0-2 g kg^{-1} drier than the rural one, depending on the time of day and date. This is not inconsistent with documented urban-rural contrasts of 0.4 g kg^{-1} for European cities (Yoshino 1975) and 0.1 g kg^{-1} for New York City in March (Clark et al. 1985). The model's specific-humidity shows urban-rural differences of about that sign and magnitude for most dates and times. The model also does well at representing the observed diurnal cycle of specific and relative humidity in terms of phase and amplitude. The JU2003 data for the three sites typically show the double maximum that is documented in the literature for specific humidity, with one in the mid-morning and one in the early evening (Geiger 1966). The model solution picks up this observed double maximum, as well as the observed daily range of 3-5 g kg^{-1}. Figure 8 shows the observed and analyzed specific humidity for 16 July, where the model greatly over-estimated the amplitude of the evening maximum at the rural site, but otherwise did reasonably well at capturing the main features of the diurnal cycle.

b. Verification of the simulated urban BL development

During JU2003, three BL wind profilers (915 MHz), from ANL, the Pacific Northwest National Laboratory (PNNL), and the University of Oklahoma (OU) operated in the central urban area of OKC (see Fig. 2 for locations of the ANL and PNNL systems). The vertical profiles of the SNR from the ANL profiler are shown in Fig. 9 for each of the eight study days, along with the model BL-height forecasts at the locations of the ANL and PNNL profilers. The SNR from the PNNL profiler is very similar to that shown

because of their proximity (6 km) and the fact that the sampled volumes of air overlap. The model reasonably simulated the urban BL in terms of the diurnal evolution of the BL height. In particular, the model nicely captured the growth rates of the convective BL from sunrise to early afternoon, as seen by comparing the slope of the model solutions and that of the SNR gradient. With some exceptions, the model also simulated well the nighttime shallow BLs, which are affected by the prevailing low-level jets (LLJs), the UHI, and the surface radiational cooling. Furthermore, the model seems to represent some of the day-to-day variation in the BL growth. For example, the difference in the growth rates on 4 July and 15 July are captured. It is worth repeating that, in the late afternoon and evening when the surface has cooled, the BL collapses but residual turbulence still exists. Thus, the maximum gradient in the SNR at this time may not indicate the BL height. Finally, it is of interest why the forecasted BL heights at the two nearby locations differ by as much as they do on some days, with the BL height at the PNNL location in the southern downtown area generally being less than at the ANL location in the northern part of the city. We speculate that the upwind PNNL location is influenced more by the shallower BL that advects into the urban area from the south. In contrast, the warm urban surface causes the simulated BL to deepen in the southerly flow, and therefore the BL is deeper in the northern part of the city.

5.3 Simulated UHI dynamics and thermodynamics

In this section, the three-dimensional (3D) structure of the UHI and its effects on the BL are analyzed using model output. Because observations are insufficient to define the 3D structure on the metropolitan-area scale, comparisons will be made with existing conceptual models of the UHI. Because the point comparisons just discussed

show that the model reasonably represents selected, observed BL features, the model-produced analyses where there are no data can be used here with some confidence.

The RTFDDA analyses on model Domain 4 for the eight clear-sky days were composited, and the surface fluxes and lower-tropospheric variables were analyzed to document the features of the UHI and the associated BL structure. Figure 10 shows that the simulated nocturnal UHI effects are prominent in the average. The 2-m AGL temperature for local midnight is about 2-3 C warmer in the urban area than in surrounding rural regions (Fig. 10a), where the shape of the thermal excess corresponds to the shape of the urbanized area. There is some downwind displacement of the warm anomaly, however. Figure 10b indicates that the simulated urban, surface, sensible-heat fluxes are less negative than in the surrounding rural area, and approach zero in some places. For individual dates, the nocturnal, urban, sensible-heat flux varies between zero and -40 W m^{-2}, which agrees well with observations taken by Grimmond et al. (2004) at a few urban locations during JU2003. Also, on a few dates there were urban regions where small upward heat fluxes prevailed for most of the night. This is consistent with the general discussion of urban surface fluxes in Grimmond and Oke (2002), and with the observation of positive nocturnal surface sensible-heat fluxes of 40 - 50 W m^{-2} at an urban site during JU2003 (Gouveia et al. 2004).

One major difference between urban and rural landscapes is that the urban surface is much drier, and there is less transpiration. The distributions of the eight-day average simulated specific humidity and relative humidity at 15 m AGL are given in Fig. 11 for 0000 LT and 1200 LT. It can be seen that the OKC urban area is characterized by a dry core, during both day and night, with a relative humidity anomaly of about 10% and a

specific humidity anomaly of about 0.5-1.5 g kg^{-1}. Obviously the relative-humidity deficit reflects the effects of both the positive temperature anomaly and the negative specific-humidity anomaly. The dry anomaly is displaced 10's of kilometers downwind.

The model simulation for 24 July illustrates an interesting possible impact of the urban area on a low-level jet (LLJ). Figure 12a shows the model-simulated BL height for 0000 LT, with rural values of about 60 m and urban-center values in excess of 250 m AGL. On this night, there existed a low-level jet, which is typical in the summer over the Great Plains (Wu and Raman 1998, Banta et al. 2002) and revealed by lidar observations during JU2003 (Wang et al. 2004; Zajic et al. 2004). The 1200 UTC sounding from OU in Norman observed a 10+ m s^{-1} speed maximum at 600 m AGL. The model analysis (Fig. 12b) shows a maximum LLJ wind speed of about 10 m s^{-1} in the rural area and < 8 m s^{-1} over the urban area. This lower speed over the city is presumably due to both the larger roughness elements and the slightly more-unstable surface layer there. The lower speeds over the city and the deeper boundary layer show characteristics similar to those of the super-critical flow and the associated compression fan observed and modeled by many (e.g., see Haack et al. 2001). The simulated wind-speed maximum is much closer to the surface than was observed, even though the low-level wind enhancement extended through a depth of over 500-m above the surface.

Large daytime differences in rural-urban BL development can also be seen. Figure 13 shows, for 1200 LT, the BL height on the 1.5-km grid (Domain 4) and cross-sections of vertical wind speed, horizontal divergence, and equivalent potential temperature. The daytime BL depth over the OKC area was 300-500 m deeper than that over rural areas (Fig. 13a), where the urban anomaly was significantly displaced

downwind (to the north) of the surface forcing. The deeper BL in the eastern part of the domain is apparently unrelated to the urban area. Also, organized mesoscale circulations develop as a result of the differential heating between the urban and rural areas (Fig. 13b,c), forming a convergence-divergence couplet in the lowest 2 km and upward motion exceeding 0.5 m s^{-1} from 1.0-1.5 km over the city. The urban anomaly in equivalent potential temperature is also apparent (Fig. 13d).

Finally, even with the simple representation of the urban area, the mesoscale model was able to simulate qualitatively reasonable features of the urban BL. Although the general properties of the simulated three-dimensional structures are conceptually consistent with results from other field experiments and previous model results (Oke 1987, Comrie 2000, Gallo and Owen 1999, Hafner and Kidder 1999), better three-dimensional observational data sets are needed for metropolitan and surrounding areas to verify these structures properly.

6. Summary and conclusions

The MM5-based mesoscale data-assimilation and forecasting system developed by NCAR for operational use at Army test ranges provided operational modeling support for the OKC JU2003 field program. In particular, the model-predicted variables were used by forecasters to help plan for intensive observation periods. Because this was an urban T&D study, of special importance was the accurate prediction of the prevailing wind field in the BL. Thus, in preparation for this model application, some known MM5 deficiencies related to the prediction of BL height and winds were corrected. This paper describes these improvements; shows the benefit to forecast skill that results, based on

pre-field-program verification studies using BL data; and then evaluates the skill of the operational system during the field program.

The model improvements involved implementation of a better representation of surface-layer momentum fluxes, a more accurate diagnosis of the BL depth, and a bulk parameterization of urban substrate properties in the LSM. Evaluation of the benefits of these changes prior to the field program showed that the well-known problem of a large negative bias in the near-surface wind speed during the day was eliminated, with daytime errors now comparable to those at night. Small improvements also resulted in the simulated near-surface temperature and wind direction during the day. In addition, profiler SNR data from Kansas indicated that the BL-height simulations were improved as well.

Then, selected operational model products available during the field program were compared with observations. Model-based analyses and forecasts of near-surface temperature and specific humidity showed reasonably accurate contrasts between urban, suburban, and rural locations. The predicted phase and range of the diurnal temperature wave was handled well, as was the more complex diurnal pattern of specific humidity. On one of the days studied, the model also reproduced what was apparently an observed nocturnal “thermal shadow” downwind of the urban area. Wind forecasts were not compared with observations from the urban area because street-canyon winds are not comparable to those from the model, which represent grid-box averages. The model BL growth rate over the city corresponded well, on most days, with that inferred from profiler SNR data.

Lastly, the model-analyzed, 3D, thermal, humidity and wind anomalies associated with the urban area were examined. Because the model forecasts verified well where data were available, it is reasonable to have some confidence in the model realizations of the 3D structures that cannot be well observed. Based on a multi-day composite, the nocturnal urban temperature was about 2.5 C warmer than that of the surrounding rural area, and the nocturnal surface heat fluxes were 20-30 W m^{-2} larger in the city. The enhanced nocturnal mixing and BL height over the city reduced the speed of a low-level jet on one night.

Perhaps one of the most interesting, and possibly surprising, implications of these results is that a mesoscale model with a simple treatment of the land-surface physics and properties can reasonably replicate the bulk effect on the BL of an urban area. This is not to say that the specific effects of buildings and street canyons, such as radiation trapping, are not important to the bulk effect of the city on the energy and moisture budgets, but that first-order effects can be represented reasonably well with simple treatments of the land surface that do not include urban-canopy models.

Acknowledgments

The development of the RTFDDA system was funded by the U.S. Army Test and Evaluation Command through an Interagency Agreement with the National Science Foundation. Support for the JU2003 operational modeling described here was provided by the Army Test and Evaluation Command and the Defense Threat Reduction Agency (DTRA). Jeff Basara's analysis of the field-program data was funded by DTRA and by National Aeronautics and Space Administration, New Investigator Award NA17RJ1277.

REFERENCES

Allwine, K. J., M. J. Leach, L. W. Stockham, J. S. Shinn, R. P. Hosker, J. F. Bowers and J. C. Pace, 2004: Overview of Joint Urban 2003 – an atmospheric dispersion study in Oklahoma City, *Symp. on Planning, Nowcasting and Forecasting in the Urban Zone*, January 11-15, Seattle, WA. Amer. Meteor. Soc.. J7.1.

Allwine K. J., J. H. Shinn, G. E. Streit, K. L. Clawson, and M. Brown, 2002: Overview of Urban 2000 – A multiscale field study of dispersion through an urban environment. *Bull. Amer. Meteor. Soc.*, **83**, 521-536.

Atkinson, B. W., 2003: Numerical modeling of urban heat-island intensity. *Bound.-Layer. Meteor.*, **113,** 285-310.

Banta, R. M., R. K. Newsom, J. K. Lundquist, Y. L. Pichugina, R. L. Coulter, and L. Mahrt, 2002: Nocturnal low-level jet characteristics over Kansas during CASE-99. *Bound.-Layer. Meteor.*, **105,** 221-252.

Beljaars, A. C. M., 1994: The parameterization of surface fluxes in large-scale models under free-convection. *Q. J. R. Meteorol. Soc*., **121**, 255-270.

Brock, F. V., K. C. Crawford, R. L. Elliott, G. W. Cuperus, S. J. Stadler, H. L. Johnson, and M. D. Eilts, 1995: The Oklahoma Mesonet: a technical overview. *J. Atmos. Oceanic Technol.*, **12**, 5-19.

Brown, M., 2000: Urban parameterization for mesoscale models, in Z. Boybey (ed.) *Mesoscale Atmospheric Dispersion*, Wessex Press, 448 pp.

Chen, F., and J. Dudhia. 2001: Coupling an advanced land surface-hydrology model with the Penn State/NCAR MM5 modeling system. Part I: model implementation and sensitivity. *Mon. Wea. Rev.*, **129**, 569-585.

Chen, F., Z. I. Janjic, and K. Mitchell, 1997: Impact of atmospheric surface-layer parameterizations in the new land-surface scheme of the NCEP mesoscale Eta model. *Bound.-Layer. Meteor.*, **85,** 391-421.

Chen, F., Y. Liu, H. Kusaka, M. Tewari, J-W Bao, 2004: Utilizing the coupled WRF/LSM/urban modeling system with detailed urban classification to simulate the urban heat island phenomena over the greater Houston area. *Preprints Fifth Urban Environment Conference,* 23-27 August, Vancouver, Canada, Amer. Meteor. Soc.

Cheng, F., D. Byun, and S. Kim, 2003: Sensitivity study of the effects of land surface characteristics on meteorological simulations during the TexAQS2000 period in the Houston-Galveston area, *13th PSU/ NCAR Mesoscale Model Users' Workshop*, June 10 -11, Boulder, CO.

Clark, E. C., R. D. Bornstein, and Y. T. Tam, 1985: Current and potential anthropogenic moisture effects on the New York City planetary boundary layer. *J. Air Pollution Control Assoc.*, **35**, 831-833.

Comrie, A. C., 2000: Mapping a wind-modified urban heat island in Tucson (with comments on integrating research and undergraduate learning). *Bull. Amer. Meteor. Soc,* **81**, 2417-2431.

Coulter, R. L., and D. H. Holdridge, 1998: A procedure for the automatic estimation of mixed layer height. *Proc. Eighth Atmospheric Radiation Measurement (ARM)*

Program Science Team Meeting, Tucson, AZ, Dept. of Energy Office of Energy Res., 177-180.

Cram, J. M., Y. Liu, S. Low-Nam, R.-S. Sheu, L. Carson, C. A. Davis, T. T. Warner, J. F. Bowers, 2001: An operational mesoscale RT-FDDA analysis and forecasting system. *Preprint, 18th Conf. Wea. Anal. For. and 14th Conf. Num. Wea. Pred.*, Ft. Lauderdale, FL. 30 July – 2 Aug., Amer. Meteor. Soc.

Deardorff, J. W., 1972: Numerical investigation of neutral and unstable planetary boundary layer. *J. Atmos. Sci.*, **29**, 91-115.

Doran, J. C., J. D. Fast, and J. Horel, 2002: The VTMX 2000 campaign. *Bull. Amer. Meteor. Soc*., **83**, 537-551.

Dupont, S., T. L. Otte, and J. K. S. Ching, 2003: Simulation of meteorological fields within and above urban and rural canopies with a mesoscale model (MM5). *Bound.-Layer. Meteor*., **113,** 111-158,

Ek, M. B., K. E. Mitchell, Y. Lin, E. Rogers, P. Grunmann, V. Koren, G. Gayno, and J. D. Tarpley, 2003: Implementation of Noah land surface model advances in the National Centers for Environmental Prediction operational mesoscale Eta model, *J. Geophys. Res*., **108**(D22), 8851.

Gallo, K. P., and T. W. Owen, 1999: Satellite-based adjustments for urban heat island temperature bias. *J. Appl. Meteor.*, **38**, 806-813.

Geiger, R., 1966: *The Climate Near the Ground*. Harvard University Press, Cambridge, 611 pp.

Gouveia, F. J., M. J. Leach, and J. H. Smith, 2004: Measurements of net radiation, ground heat flux and surface temperature in an urban canyon. *Symp. on Planning,*

Nowcasting, and Forecasting in the Urban Zone, Seattle, WA, 11-15 January, Amer. Meteor. Soc.. J7.4.

Grell, G., J. Dudhia and D. Stauffer, 1993: A description of the Fifth-Generation Penn State/NCAR Mesoscale Model (MM5). *NCAR/TN-398+STR*, Boulder, CO.

Grimmond, C. S. B., and T. R. Oke, 2002: Turbulent heat fluxes in urban areas: observations and local-scale urban meteorological parameterization scheme (LUMPS). *J. Appl. Meteor*., **41**, 792-810.

Grimmond, C. S. B., H.-B. Su, B. Offerle, B. Crawford, S. Scott, S. Zhong, and C. Clements, 2004: Variability of sensible heat fluxes in a suburban area of Oklahoma City. *Symp. on Planning, Nowcasting, and Forecasting in the Urban Zone*, Seattle, WA, 11-15 January, Amer. Meteor. Soc.. J7.2.

Grossman-Clarke, S., J. A. Zehnder, W. L. Stefanov, Y. Liu, and M. A. Zoldak, 2005: Urban modifications in a mesoscale meteorological model and the effects on near surface variables in an arid metropolitan region, *J. Appl. Meteor*. (in press).

Haack, T, S. D. Burk, C. Dorman and D. Rogers, 2001: Supercritical flow interaction within the Cape Blanco-Cape Mendocino orographic complex. *Mon. Wea. Rev.*, **129**, 688-708.

Hafner, J., and S. Q. Kidder, 1999: Urban heat island modeling in conjunction with satellite-derived surface/soil parameters. *J. Appl. Meteor.*, **38**, 448-465.

Holt T., D. Niyogi , F. Chen, M. A. LeMone, K. Manning, A. L. Qureshi, 2005: Effect of Land - Atmosphere Interactions on the IHOP 24-25 May 2002 Convection Case, *Monthly Weather Review*, (IHOP Special Issue), in press.

Hong, S.-Y., and H.-L. Pan, 1996: Non-local boundary layer vertical diffusion in a Medium-Range Forecast model. *Mon. Wea. Rev*., **124**, 2322-2339.

Kusaka H., H. Kondo, Y. Kikegawa, and F. Kimura, 2001: A simple single-layer urban canopy model for atmospheric models: comparison with multi-layer and slab models. *Bound.-Layer Meteor*., **101**, 329-358

Liu, Y., S. Low-Nam, R.-S. Sheu, L. Carson, C. A. Chris, T. T. Warner, S. P. Swerdlin, J. F. Bowers, M. Xu, H.-M. Hsu, and D. L. Rife, 2002: Performance and enhancements of the NCAR/ATEC mesoscale FDDA and forecasting system. *15th Conf. on Num. Wea. Pred.*, San Antonio, Taxes, 12-16 August, Amer. Meteor. Soc., 399-402.

LeMone M. A, R. L. Grossman, R. L. Coulter, M. L. Wesley, G. E. Klazura, G. S. Poulos, W. Blueman, J. K. Lundquist, R. H. Cuenca, S. F. Kelly, E. A. Brandes, S. P. Oncley, R. T. McMillen and B. B. Hicks, 2000: Land-atmosphere interaction research, early results and opportunities in the Walnut River Watershed in southeast Kansas: CASE and ABLE. *Bull. Amer. Meteor. Soc*., **8**, 757-779.

Martilli, A., A. Clappier, and M. W. Rotach, 2002: An urban surface exchange parameterization for mesoscale models. *Bound.-Layer Meteor*., **104**, 261-304.

Masson, V., 2000: A physically-based scheme for the urban energy budget in atmospheric models. *Bound.-Layer Meteor*., **94**, 357-397.

Niyogi D., S. Raman S., and K. Alapaty, 1999: Uncertainty in specification of surface characteristics, Part ii: Hierarchy of interaction - explicit statistical analysis Boundary Layer Meteorology, 91 , 341-366.

Oke, T. R., 1987: *Boundary Layer Climates*, 2nd ed., Routledge, London and John Wiley& Sons, New York, 435pp.

Otte, T. L., A. Lacser, S. Dupont, and J. K. S. Ching, 2004: Implementation of an urban canopy parameterization in a mesoscale meteorological model. *J. Appl. Meteor.*, **43**, 1648–1665.

Pielke, R. A., 1984: *Mesoscale Meteorological Modeling*. Academic Press, 612pp.

Stauffer, D. R., and N. L. Seaman, 1994: Multiscale four-dimensional data assimilation. *J. Appl. Meteor.*, **33**, 416-434.

Rotach, M. W., 1995: Profiles of turbulence statistics in and above an urban street canyon. *Atmos. Environ.*, **29**, 1473-1486.

Sykes, R. I., D. S. Henn, and W. S. Lewellen, 1993: Surface-layer description under free-convection conditions. *Q. J. R. Meteorol. Soc*., **119**, 409-421.

Taha, H., 1999: Modifying a mesoscale meteorological model to better incorporate urban heat storage: a bulk-parameterization approach. *J. Appl. Meteor.*, **38**, 466–273.

Uno, I., H. Ueda, and S. Wakamatsu, 1989: Numerical modeling of nocturnal urban boundary layer. *Bound.-Layer Meteor*., **49**, 77-98.

Wang, Y., D. Ligon, E. Creegan, C. Williamson, C. Klipp, M. Felton, and R. Calhoun, 2004: Turbulence characteristics over an urban domain observed by Doppler lidars. 16*th Symp. On Boundary Layers and Turbulence. 8-13* Aug. 2004, Portland, Maine. Amer. Meteor. Soc.

Wu, Y., and S. Raman, 1998: The summertime Great Plains lower level jet and the eefect of its origin on moisture transport. *Bound.-Layer Meteorol*., **88**, 445-466.

Yoshino, M. M., 1975: *Climate in a Small Area*. University of Tokyo Press, Tokyo, 549 pp.

Zajic, D., H. J. S. Fernado, M. Princevac, and R. Calhoun, 2004: Flow and turbulence in urban canopies. *5th Conf. on Urban Environment*, 22-26 Aug. 2004, Vancouver, BC. Amer. Meteor. Soc.. 6.2.

Zhang, D.-L., and R. A. Anthes, 1982: A high-resolution model of the planetary boundary layer—sensitivity tests and comparisons with SESAME-79 data. *J. Appl. Meteor*, **21**, 1594–1609.

Zhang, D.-L., and W. Zheng, 2004: Diurnal cycles of surface winds and temperatures as simulated by five boundary-layer parameterizations. *J. Appl. Meteor.*, **43**, 157-169.

Zilitinkevich, S., 1995: Non-local turbulent transport: pollution dispersion aspects of coherent structure of convective flows. *Air Pollution III -Volume I: Air Pollution Theory and Simulation* (Eds., H. Power, N. Moussiopoulos and C. A. Brebbia). Computational Mechanics Publications, Southampton Boston, 53-60.

Table 1: Comparison of simulated and observed 10-m temperature differences between urban (PW14) and rural (MINC) locations and between urban and suburban (SPEN) locations at the designated times, and the range in the diurnal temperature variation at the three stations. The observations are to the right of the slashes, and the simulated values are to the left. (7/24, the date with easterly winds, is not included in the mean in the bottom row).

Dates	**Temperature differences (C)**				**Diurnal temperature range (C)**		
	PW14 – MINC		**PW14 - SPEN**		**PW14**	**SPEN**	**MINC**
	0600 LT	1400 LT	0600 LT	1400 LT			
7/04	2.5/2.9	2.0/2.1	0.9/1.2	1.9/2.0	10.3/9.8	9.8/9.2	10.7/10.0
7/05	1.8/2.4	2.7/2.4	0.6/0.9	1.2/1.1	10.1/9.2	9.6/9.0	9.7/9.9
7/15	2.1/1.9	2.0/0.8	0.3/0.2	1.1/0.8	10.2/10.0	9.8/9.1	10.8/11.6
7/16	3.7/3.1	2.4/2.2	0.8/1.7	2.0/2.3	11.0/10.9	9.5/11.4	12.0/12.6
7/17	3.1/3.2	2.7/2.1	0.2/1.3	2.0/0.6	11.0/10.4	9.3/10.8	12.1/12.0
7/18	2.8/3.0	2.6/2.0	0.5/1.8	1.7/0.8	13.1/11.8	10.1/10.9	13.3/13.0
7/24	0.2/2.0	1.7/0.7	2.3/2.9	1.9/0.7	13.9/12.8	14.6/15.0	13.4/13.3
7/25	1.8/2.1	2.0/0.5	1.8/1.6	1.2/0.5	10.9/11.2	10.5/12.1	10.4/11.6
Mean	**2.54/2.65**	**2.05/1.72**	**0.72/1.24**	**1.60/1.15**	**10.94/10.47**	**9.80/10.35**	**11.28/11.52**

Figure captions

Figure 1. Bias errors of 10-m AGL wind speed for 10-12 h forecasts on the fine mesh of a nested grid (either 1.1 or 3.3 km grid increment). These are averaged statistics for five Army test ranges, as verified against the range observations (71 mesonet stations) during August 2002. Plots are shown for Cold Regions Test Center, Alaska (CRTC), Dugway Proving Ground, Utah (DPG), White Sands Missile Range, New Mexico (WSMR), Yuma Proving Ground, Arizona (YPG), and Aberdeen Test Center, Maryland (ATC).

Figure 2. The RTFDDA grid configuration, terrain height in Domain 1, and land use on Domain 4. The urban areas (gray shades in Domains 4 and 5) of OKC and Norman are shown. The A and P symbols indicate the locations of the ANL and PNNL profilers, respectively. The M, S and W symbols show the locations of three surface stations used in the model verification: Oklahoma mesonet stations MINC and SPEN, and the Dugway Proving Ground PWIDS 14, respectively.

Figure 3. The signal-to-noise ratio (color) for the ANL 915-MHz wind profilers in Beaumont (upper), Whitewater (middle), and Oxford (bottom) Kansas, observed from 1800 LT 27 May to 1800 LT 28 May 2003. Superimposed are the BL heights of the RTFDDA 0-13 hour forecasts beginning at 0500 local time, interpolated to the profiler locations, with the old (black) and new (red) surface-layer physics and BL-height-diagnosis schemes.

Figure 4. Comparison of old and new MRF BL schemes for the period 0000 UTC 27 May to 0000 UTC 29 May 2003 in terms of bias (a) and RMS (b) errors for analyses (Anal) and 10-12 h forecasts (f10-12) of 10-m AGL wind speed, based on over 1400 METAR and other observations on model Domain 1. Forecasts were initiated every 3 h over the period. Values were interpolated from the model grid to the locations of the observations. Because a 48-h period is used for verification, each data point on the abscissa represents an average of two analyses or forecasts that are valid at that time of day. The verification is performed by horizontally interpolating the model output to the observation locations, and using similarity theory to extrapolate downward from the lowest model computation level at ~15 m AGL to the level of the observation.

Figure 5. Same as Fig. 4, but for 10-m AGL wind direction and 2-m AGL temperature RMS errors.

Figure 6. Comparison of monthly mean 10-m AGL wind speed bias and RMS errors of analyses (Anal) and 4 – 6 hour forecasts (f4-6) from a 10-km grid-increment grid of the operational mesoscale forecasting system at the ATEC Aberdeen Test Center, Maryland for August 2002, before the MRF physics changes were made, and for August 2003, after they were made. The verification is performed by horizontally interpolating the model output to the observation locations, and using similarity theory to extrapolate downward from the lowest model computation level at ~15 m AGL to the level of the observation.

Figure 7. The diurnal evolution of the observed (right panels) and model-analyzed (left panels) ~10-m AGL temperatures at the urban, rural, and suburban stations for 16

July (southerly flow) and 24 July (easterly flow) 2003. The verification results for the other six clear-sky days are generally similar to those for the 16 July case. Note that PW14 observations are at 10 m AGL while MINC and SPEN observations are at 9 m AGL. Model values are obtained at the observation locations by horizontally interpolating the model output to the observation locations, and using similarity theory to extrapolate downward from the lowest model computation level at ~15 m AGL to the level of the observation.

Figure 8. Same as Fig. 7, but for specific humidity; 16 July case only.

Figure 9. Vertical profiles of the SNR from the ANL profiler for each of the eight study days, with the model-analyzed BL-height at the locations of the ANL (red) and PNNL (black) profilers.

Figure 10. Composite 2-m AGL temperature (a: C) and surface sensible heat flux (b: W m^{-2}), based on RTFDDA analyses, for the nine clear-sky days in July 2003, valid at 0000 LT. The isopleth interval for temperature in (a) is 0.5 C and for sensible heat flux in (b) is 10 W m^{-2}. Model temperatures are obtained at 2 m AGL by using similarity theory to extrapolate downward from the lowest model computation level at ~15 m AGL. The OKC urban area is marked with thick solid lines.

Figure 11. Mean 2-m AGL relative humidity (a, c, isopleth interval is 5%) and specific humidity (b, d, isopleth interval is 0.5 g kg^{-1}) at 0000 LT (a, b) and 1200 LT (c, d), based on RTFDDA analyses. Model humidities are obtained at 2 m AGL by using similarity theory to extrapolate downward from the lowest model computation level at ~15 m AGL. The OKC urban area is marked with thick solid lines.

Figure 12. For 0000 LT 24 July 2003, RTFDDA-analyzed BL height on Domain 4 (1.5-km grid increment, a), and wind speed perpendicular to the cross section AB. The isopleth interval for BL height in (a) is 20 m and the interval of wind speed in (b) is 1 m s^{-1}. The OKC urban area is marked with thick solid lines in (a).

Figure 13. For 1200 LT 5 July 2003, RTFDDA-analyzed BL height on Domain 4 (1.5-km grid increment (a, isopleth interval of 150 m) and vertical cross sections of vertical motion (b, isopleth interval of 0.1 m s^{-1}), horizontal divergence (c, isopleth interval of $10x10^{-5}$ s^{-1}) and θe (d, isopleth interval of 2 K) along the line AB in panel (a). The OKC urban area is marked with thick solid lines in (a). The approximate extent of the urban area is indicated in the cross sections.

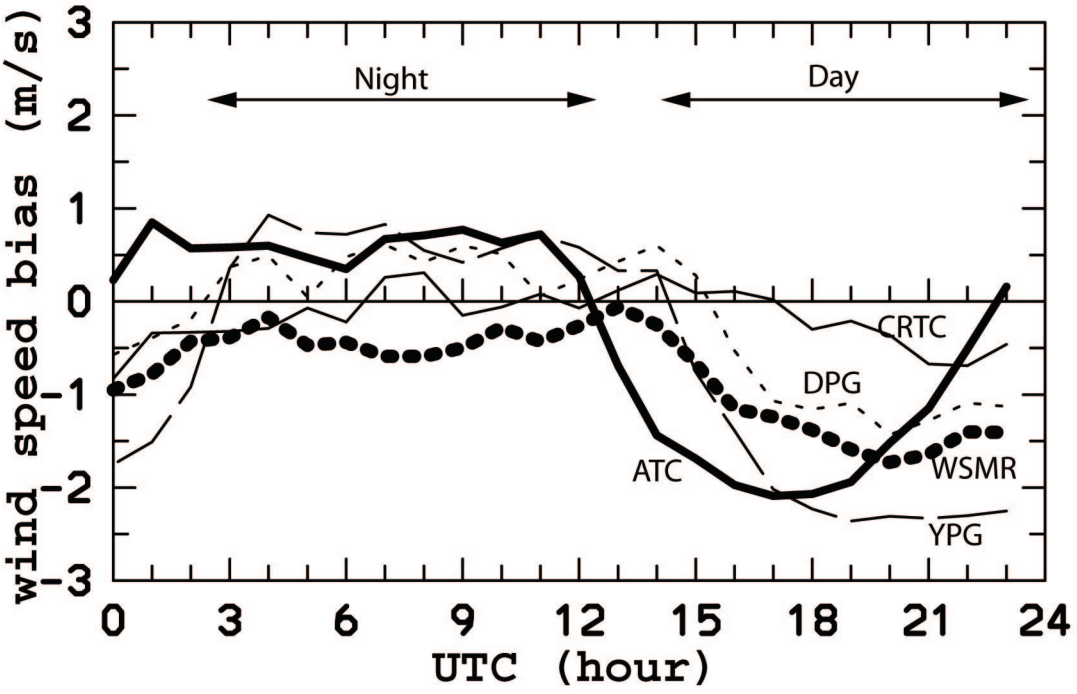

Figure 1. Bias errors of 10-m AGL wind speed for 10-12 h forecasts on the fine mesh of a nested grid (either 1.1 or 3.3 km grid increment). These are averaged statistics for five Army test ranges, as verified against the range observations (71 mesonet stations) during August 2002. Plots are shown for Cold Regions Test Center, Alaska (CRTC), Dugway Proving Ground, Utah (DPG), White Sands Missile Range, New Mexico (WSMR), Yuma Proving Ground, Arizona (YPG), and Aberdeen Test Center, Maryland (ATC).

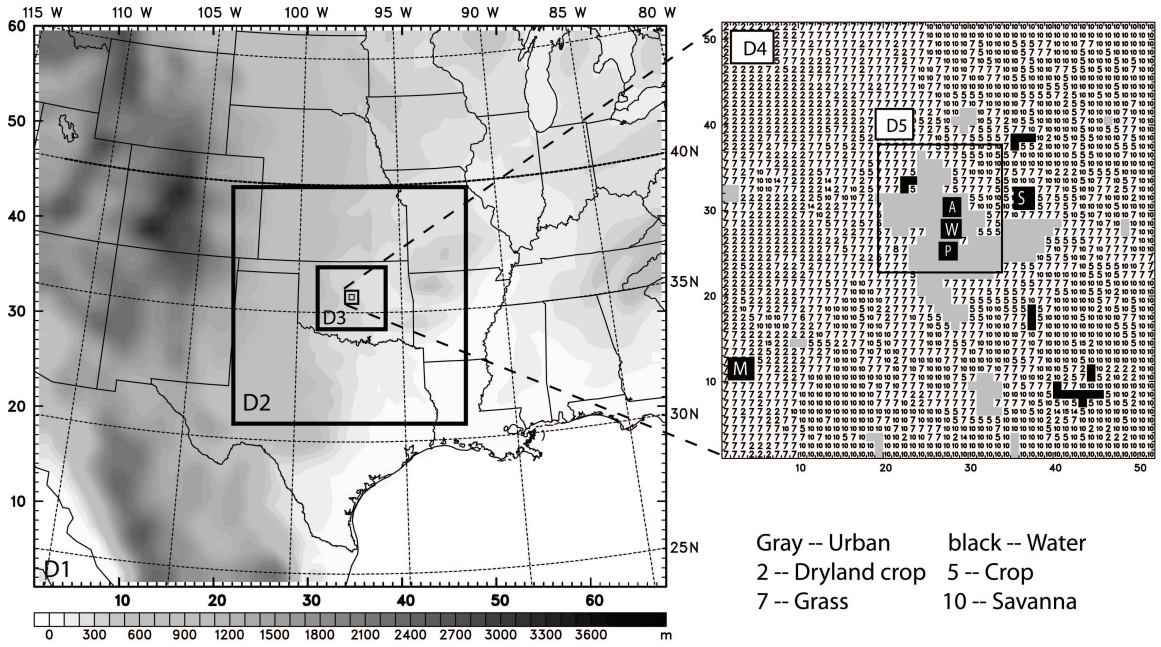

Figure 2. The RTFDDA grid configuration, terrain height in Domain 1, and land use on Domain 4. The urban areas (gray shades in Domains 4 and 5) of OKC and Norman are shown. The A and P symbols indicate the locations of the ANL and PNNL profilers, respectively. The M, S and W symbols show the locations of three surface stations used in the model verification: Oklahoma mesonet stations MINC and SPEN, and the Dugway Proving Ground PWIDS 14, respectively.

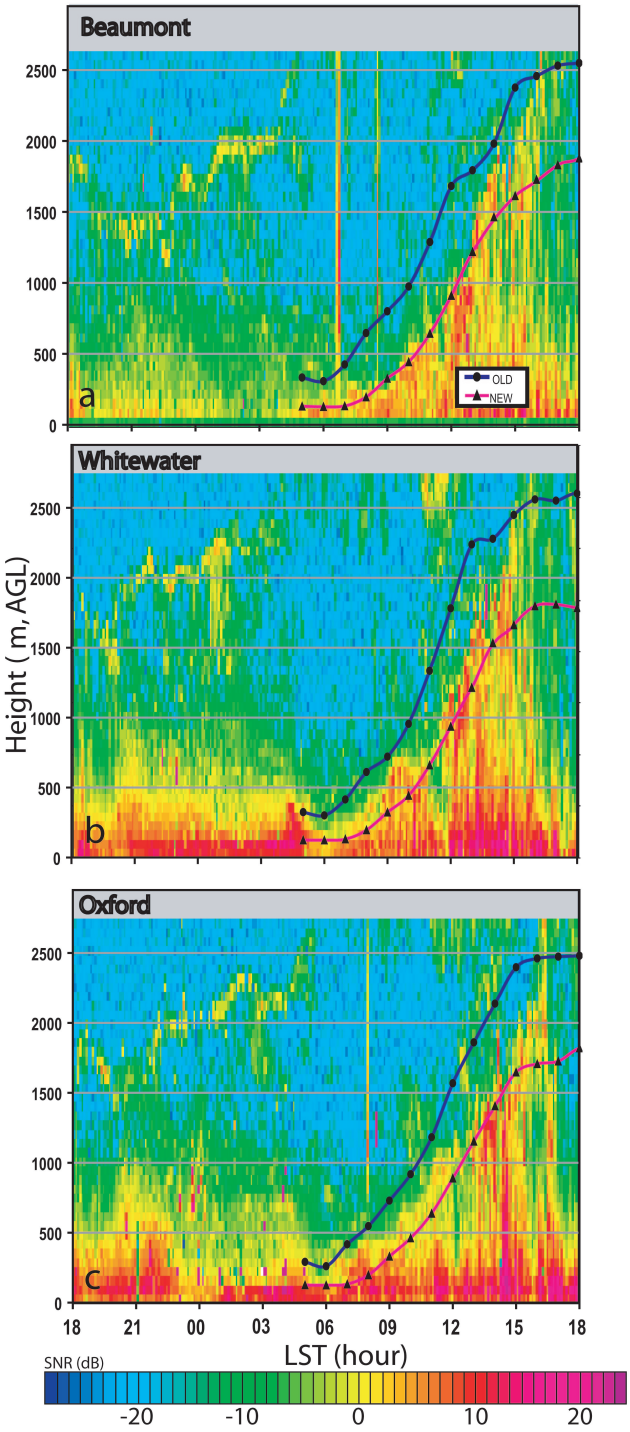

Figure 3. The signal-to-noise ratio (color) for the ANL 915-MHz wind profilers in Beaumont (upper), Whitewater (middle), and Oxford (bottom) Kansas, observed from 1800 LT 27 May to 1800 LT 28 May 2003. Superimposed are the BL heights of the RTFDDA 0-13 hour forecasts beginning at 0500 local time, interpolated to the profiler locations, with the old (black) and new (red) surface-layer physics and BL-height-diagnosis schemes.

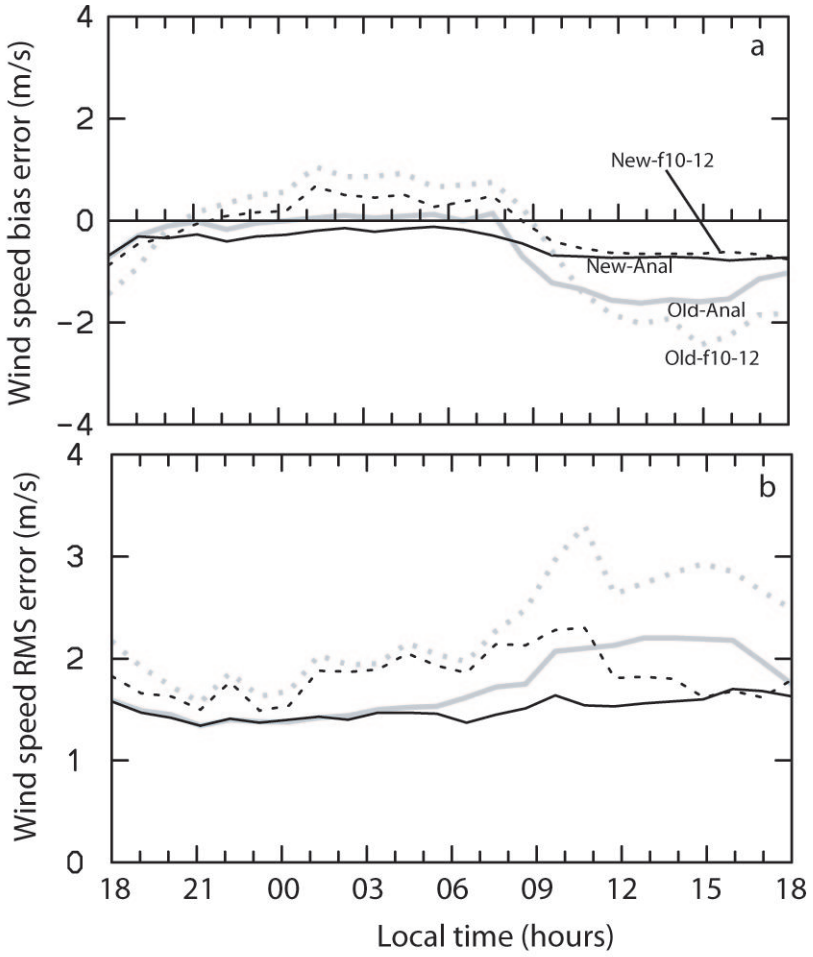

Figure 4. Comparison of old and new MRF BL schemes for the period 0000 UTC 27 May to 0000 UTC 29 May 2003 in terms of bias (a) and RMS (b) errors for analyses (Anal) and 10-12 h forecasts (f10-12) of 10-m AGL wind speed, based on over 1400 METAR and other observations on model Domain 1. Forecasts were initiated every 3 h over the period. Values were interpolated from the model grid to the locations of the observations. Because a 48-h period is used for verification, each data point on the abscissa represents an average of two analyses or forecasts that are valid at that time of day. The verification is performed by horizontally interpolating the model output to the observation locations, and using similarity theory to extrapolate downward from the lowest model computation level at ~15 m AGL to the level of the observation.

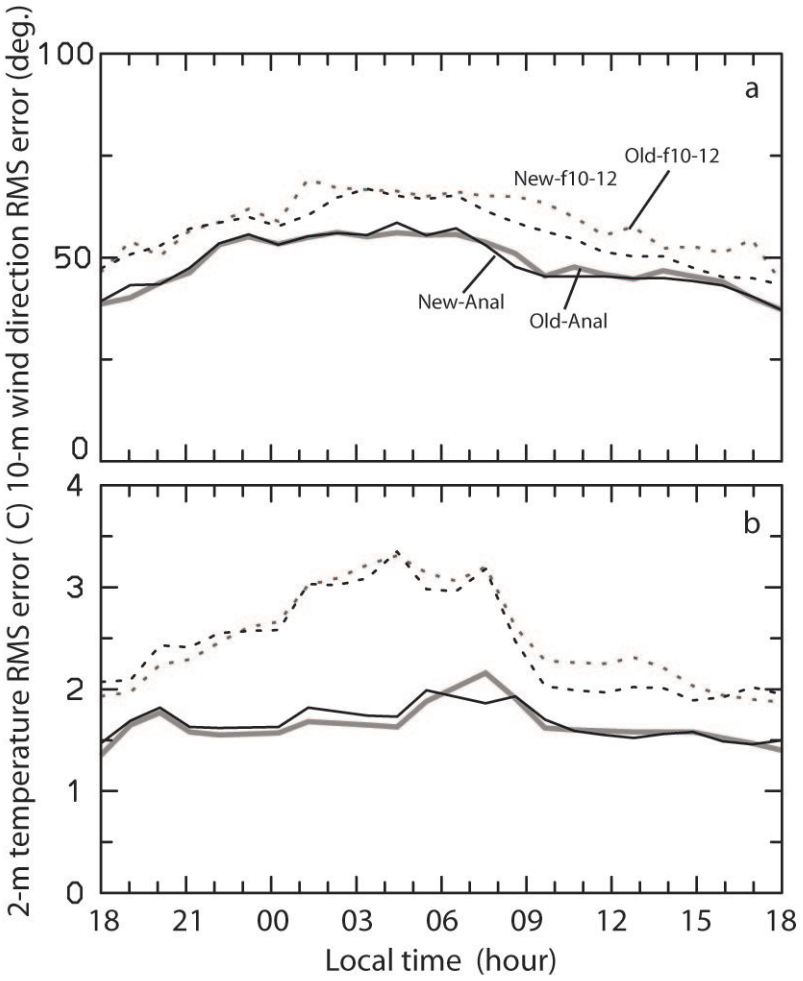

Figure 5. Same as Fig. 4, but for 10-m AGL wind direction and 2-m AGL temperature RMS errors.

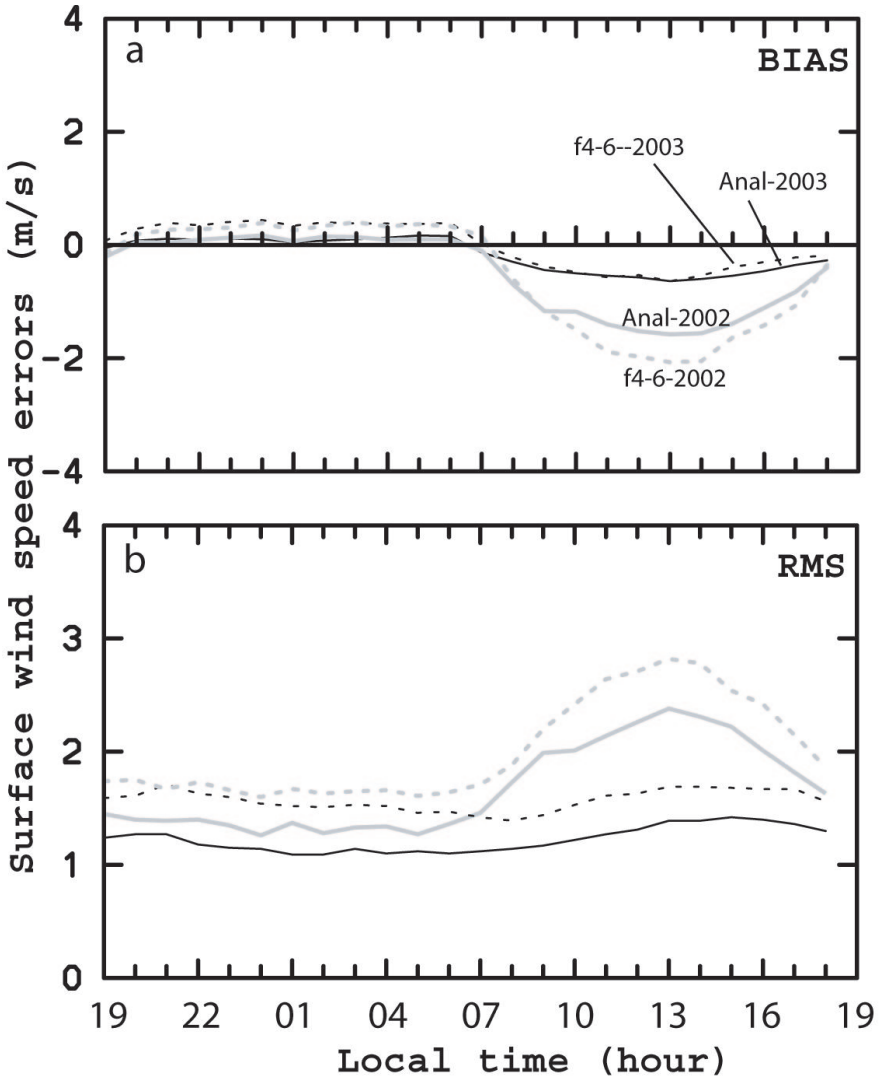

Figure 6. Comparison of monthly mean 10-m AGL wind speed bias and RMS errors of analyses (Anal) and 4 – 6 hour forecasts (f4-6) from a 10-km grid-increment grid of the operational mesoscale forecasting system at the ATEC Aberdeen Test Center, Maryland for August 2002, before the MRF physics changes were made, and for August 2003, after they were made. The verification is performed by horizontally interpolating the model output to the observation locations, and using similarity theory to extrapolate downward from the lowest model computation level at ~15 m AGL to the level of the observation.

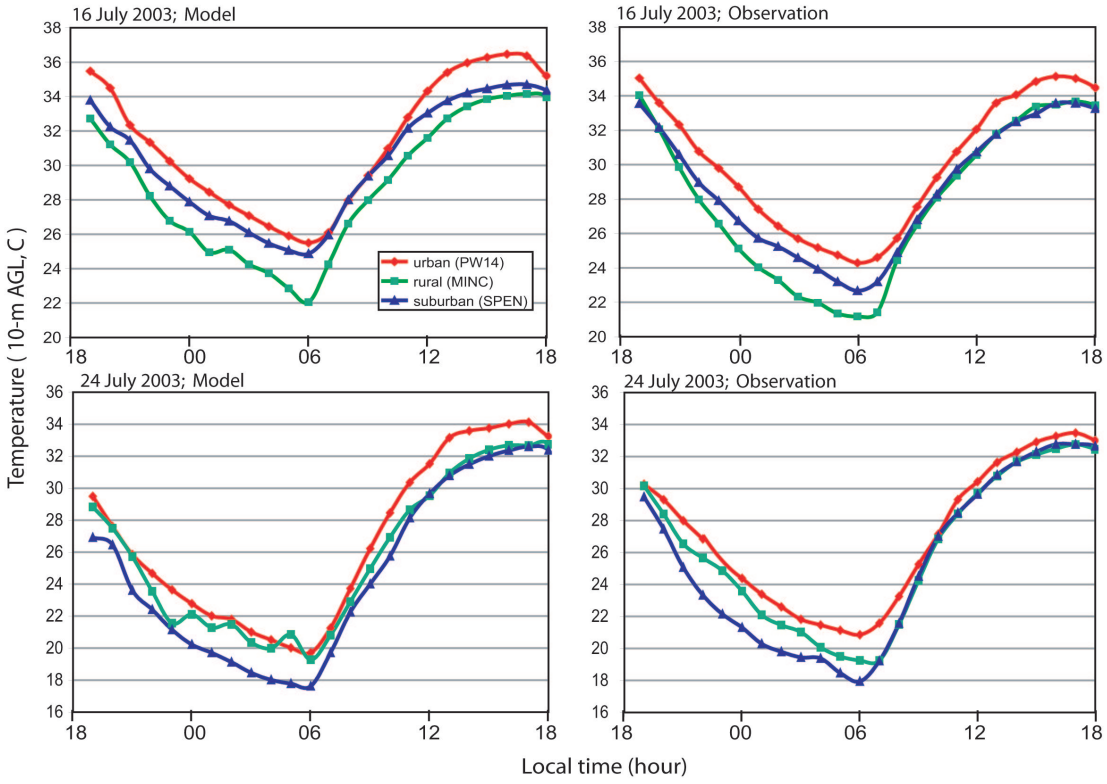

Figure 7. The diurnal evolution of the observed (right panels) and model-analyzed (left panels) ~10-m AGL temperatures at the urban, rural, and suburban stations for 16 July (southerly flow) and 24 July (easterly flow) 2003. The verification results for the other six clear-sky days are generally similar to those for the 16 July case. Note that PW14 observations are at 10 m AGL while MINC and SPEN observations are at 9 m AGL. Model values are obtained at the observation locations by horizontally interpolating the model output to the observation locations, and using similarity theory to extrapolate downward from the lowest model computation level at ~15 m AGL to the level of the observation.

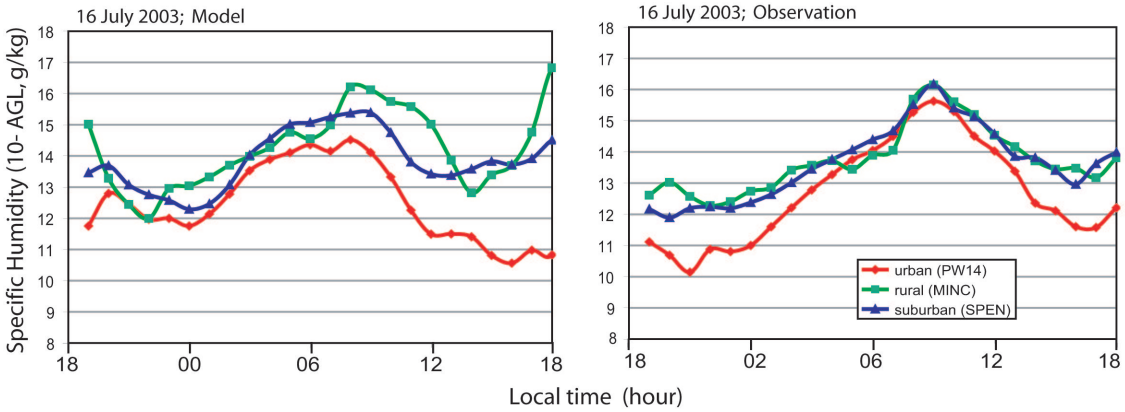

Figure 8. Same as Fig. 7, but for specific humidity; 16 July case only.

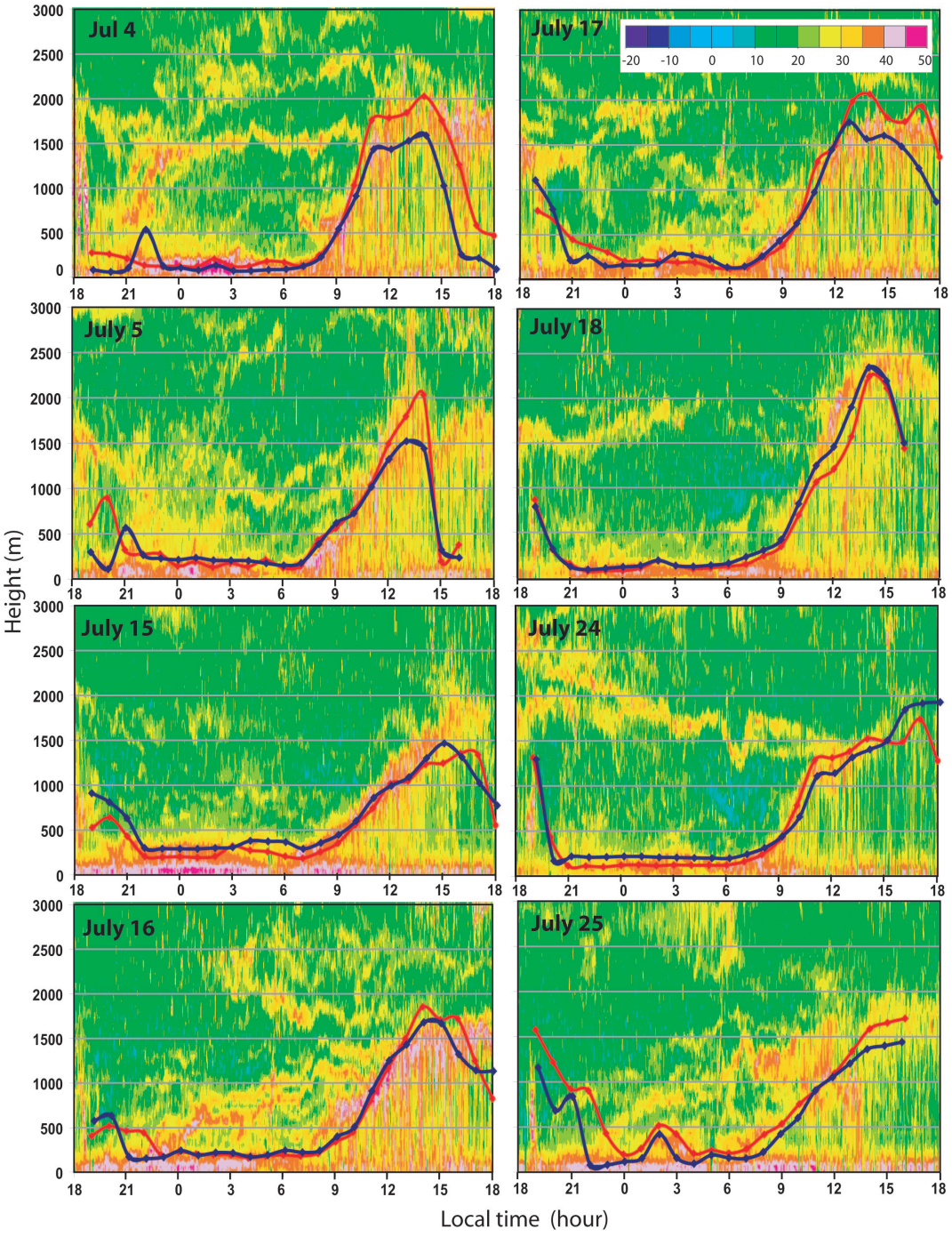

Figure 9. Vertical profiles of the SNR from the ANL profiler for each of the eight study days, with the model-analyzed BL-height at the locations of the ANL (red) and PNNL (black) profilers.

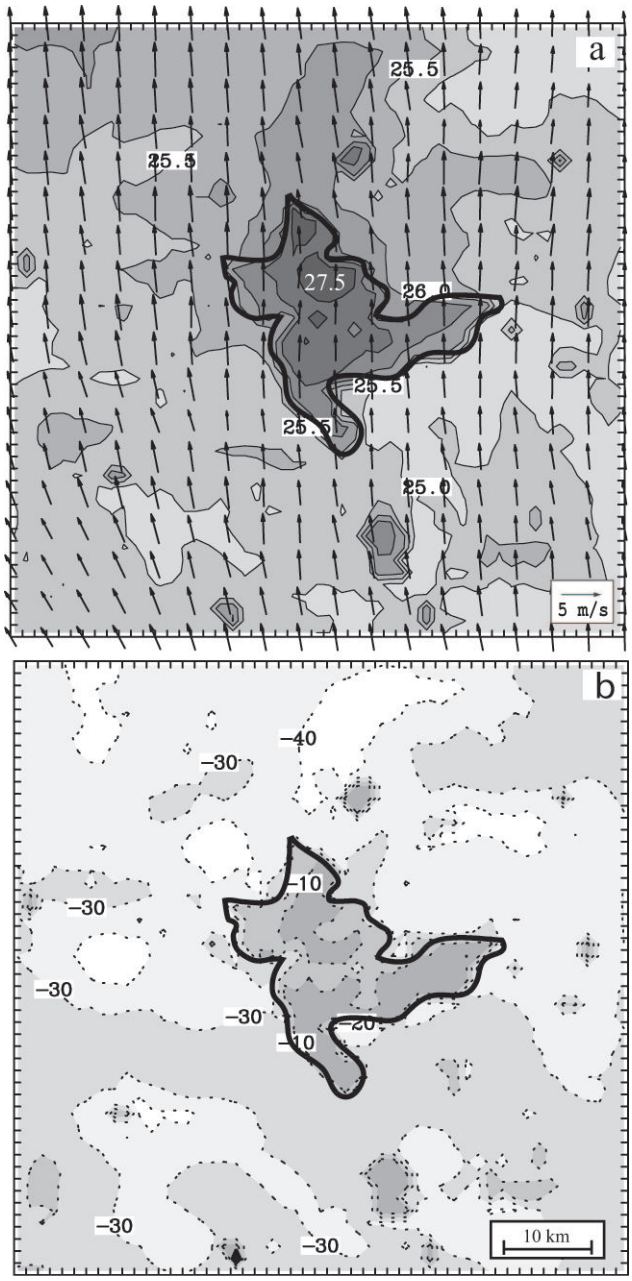

Figure 10. Composite 2-m AGL temperature (a: C) and surface sensible heat flux (b: W m-2), based on RTFDDA analyses, for the nine clear-sky days in July 2003, valid at 0000 LT. The isopleth interval for temperature in (a) is 0.5 C and for sensible heat flux in (b) is 10 W m-2. Model temperatures are obtained at 2 m AGL by using similarity theory to extrapolate downward from the lowest model computation level at ~15 m AGL. The OKC urban area is marked with thick solid lines.

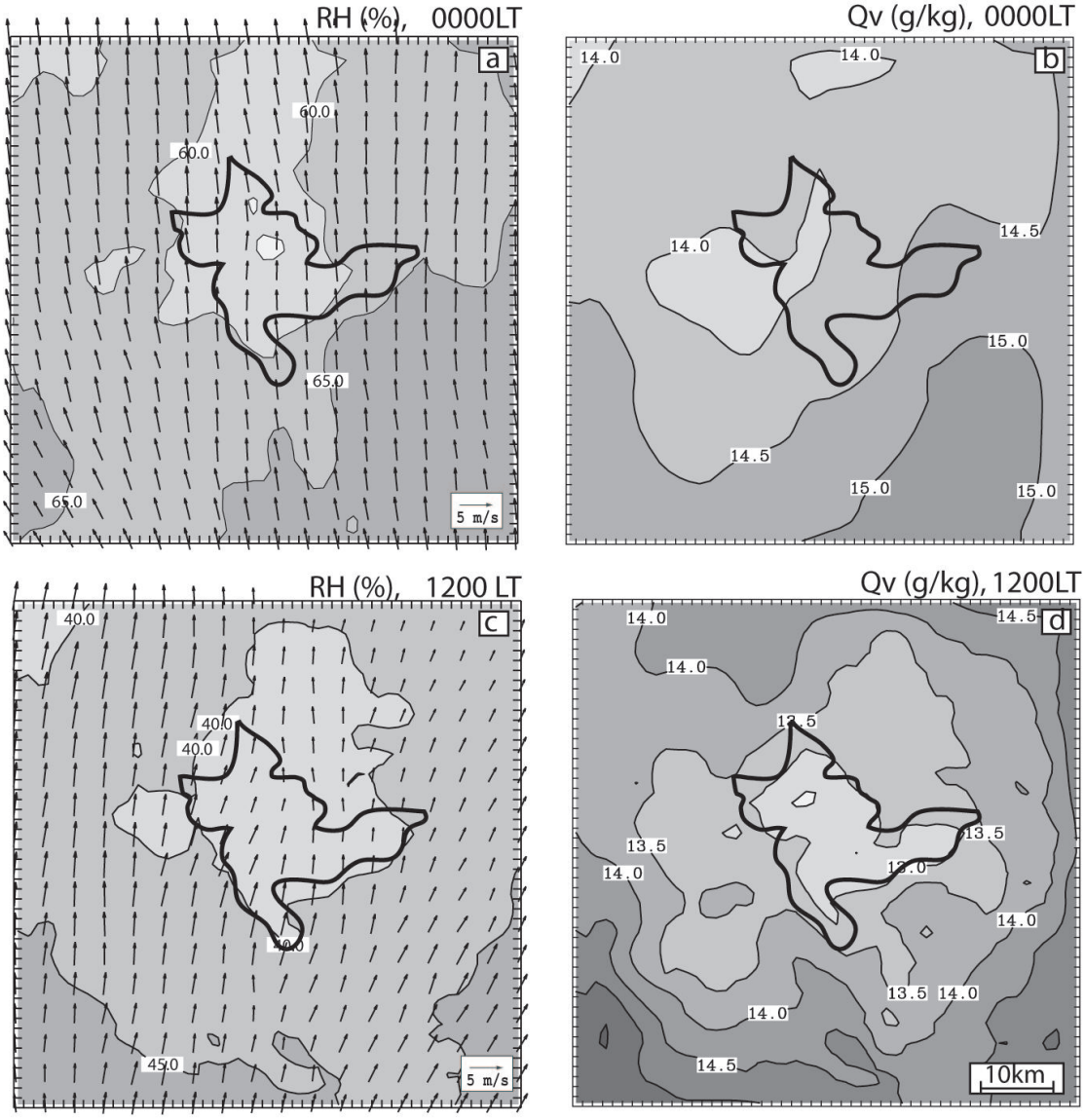

Figure 11. Mean 2-m AGL relative humidity (a, c, isopleth interval is 5%) and specific humidity (b, d, isopleth interval is 0.5 g kg-1) at 0000 LT (a, b) and 1200 LT (c, d), based on RTFDDA analyses. Model humidities are obtained at 2 m AGL by using similarity theory to extrapolate downward from the lowest model computation level at ~15 m AGL. The OKC urban area is marked with thick solid lines.

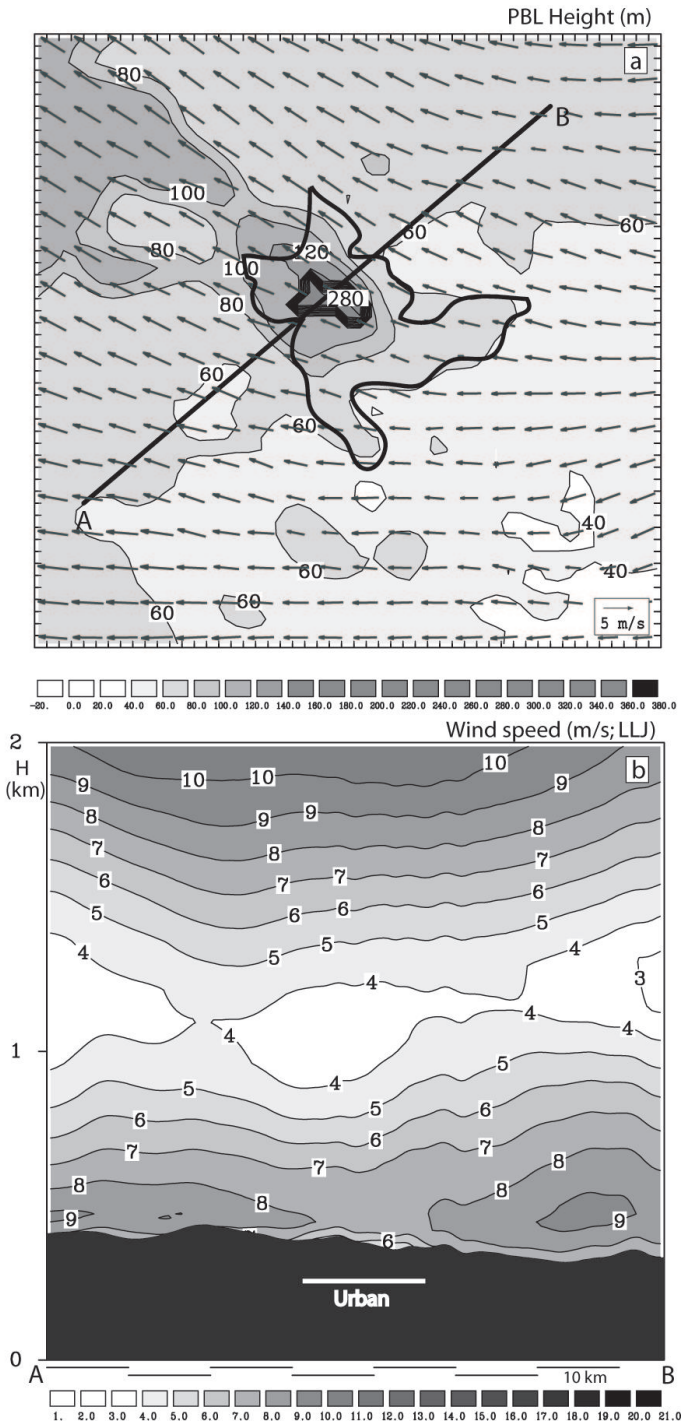

Figure 12. For 0000 LT 24 July 2003, RTFDDA-analyzed BL height on Domain 4 (1.5-km grid increment, a), and wind speed perpendicular to the cross section AB. The isopleth interval for BL height in (a) is 20 m and the interval of wind speed in (b) is 1 m s-1. The OKC urban area is marked with thick solid lines in (a).

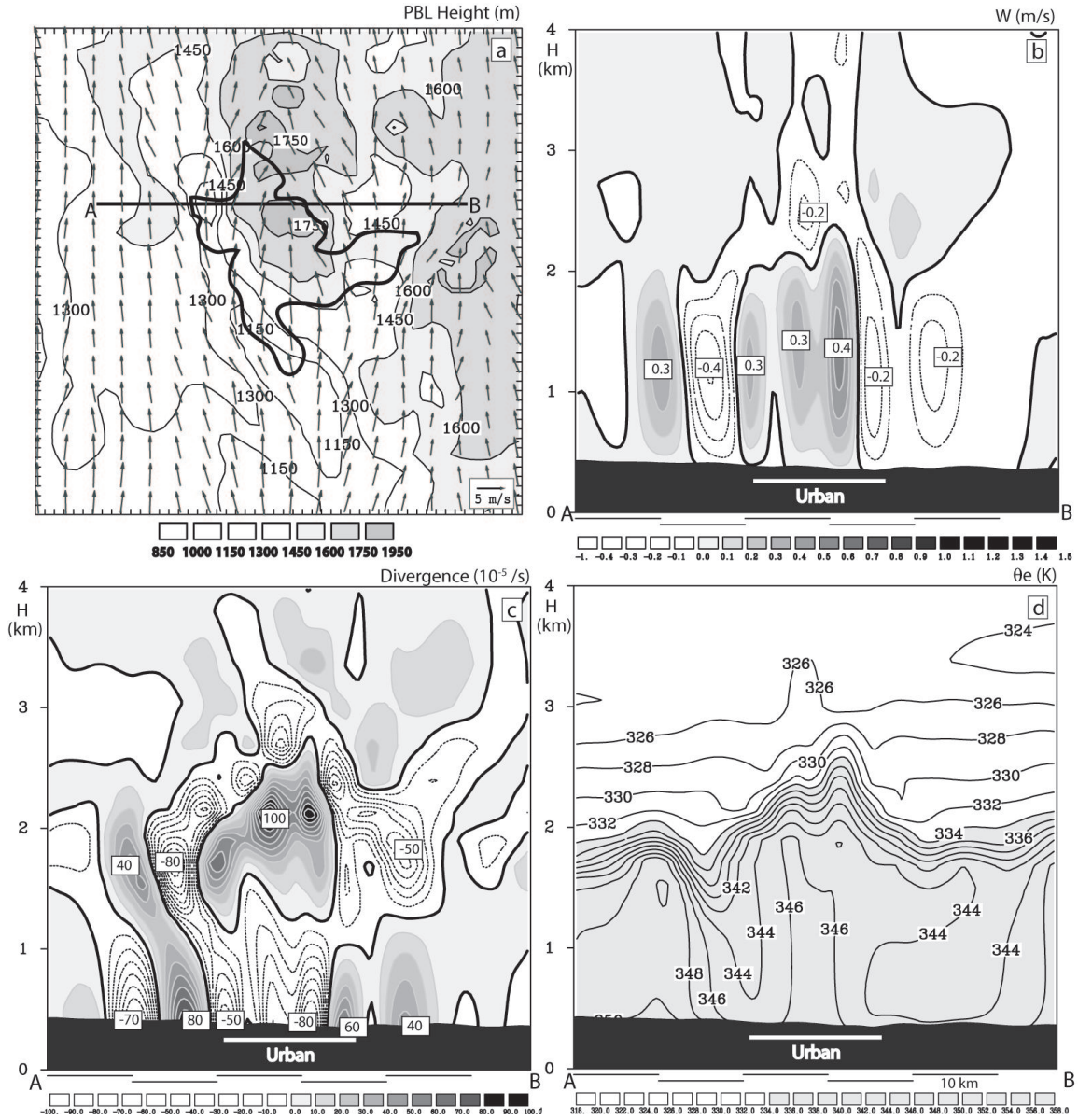

Figure 13. For 1200 LT 5 July 2003, RTFDDA-analyzed BL height on Domain 4 (1.5-km grid increment (a, isopleth interval of 150 m) and vertical cross sections of vertical motion (b, isopleth interval of 0.1 m s-1), horizontal divergence (c, isopleth interval of 10x10-5 s-1) and θε (d, isopleth interval of 2 K) along the line AB in panel (a). The OKC urban area is marked with thick solid lines in (a). The approximate extent of the urban area is indicated in the cross sections.